THE PENNSYLVANIA STATE UNIVERSITY
SCHREYER HONORS COLLEGE

DEPARTMENT OF ASTRONOMY AND ASTROPHYSICS

COMPOSITE SPECTRA OF LYMAN-ALPHA EMITTING GALAXIES FROM THE HOBBY-EBERLY TELESCOPE DARK ENERGY EXPERIMENT

ADAM MCCARRON
SPRING 2019

A thesis
submitted in partial fulfillment
of the requirements
for baccalaureate degrees
in Astronomy and Astrophysics and Physics
with honors in Astronomy and Astrophysics

Reviewed and approved* by the following:

Robin Ciardullo
Professor of Astronomy and Astrophysics
Thesis Supervisor

Jane Charlton
Professor of Astronomy and Astrophysics
Honors Adviser

* Signatures are on file in the Schreyer Honors College.

ABSTRACT

The ability to translate the wavelength of a Lyman-alpha emission line detection into a redshift that can be used for cosmological calculations serves as a vital step in achieving HETDEX science goals. In this analysis, I use a composite spectrum of ~10,000 Lyman-alpha emitting galaxies (LAEs) in a redshift range of $1.9 < z < 3.5$ to attempt to measure a systematic offset of the Lyman-alpha emission line from interstellar absorption lines. This offset would affect the redshift estimates from detections of single emission lines and improve the accuracy of calculations of cosmological parameters. The presence of [OII]λ3727 emitting galaxies in the sample prevented the weak LAE features from appearing convincingly in the composite spectra, but improvements being made to the HETDEX detection algorithm and interloper discrimination will allow the measurement to be made in the near future using the analysis presented in this thesis.

TABLE OF CONTENTS

LIST OF FIGURES

LIST OF TABLES

ACKNOWLEDGEMENTS

I would like to thank Robin Ciardullo for his support and guidance throughout my entire undergraduate experience as a researcher. I would also like to thank Penn State's HETDEX team for their illuminating insights and useful advice over the years. I thank Jane Charlton for her feedback on this project. Finally, I am grateful for my mom, dad and brother, because I could not have gotten where I am today without their steadfast love and enthusiastic encouragement.

Chapter 1

Introduction

The Hobby-Eberly Telescope Dark Energy Experiment (HETDEX) will map roughly one million galaxies in the early universe in order to measure its expansion history and constrain the evolution of dark energy. This chapter will discuss the survey design, the instrument, and the observations and theory pertaining to how the light it detects escapes from a distant galaxy.

The HETDEX Survey

The survey, recently underway, uses the Visible Integral-field Replicable Unit Spectrograph (VIRUS) illuminated by the Hobby-Eberly Telescope's ten-meter effective aperture mirror. It will detect roughly 0.8 million Lyman-alpha emitting galaxies (LAEs), named after the photon produced when an electron transitions from the first excited state to the ground state in hydrogen, in order to use their positions to understand how dark energy shapes the expansion history of the universe. It will cover a patch of 420 $\deg^2$ to observe redshifted Lyman-alpha emission between 350 and 550 nm corresponding to a redshift range of $1.9 < z < 3.5$ (Hill et al 2007). The instrument consists of 150 individual integral field unit (IFU) spectrographs each fed by 246 fibers with diameters covering 4.16" on the sky and a fill factor of one-third. The spectrographs achieve resolving powers of R∼850 over the full wavelength coverage (Hill et al. 2008).

The survey seeks to break ground in cosmology by placing tight constraints on the crucial parameters that dictate how the universe evolves over time. Currently, astronomers do not definitively know how dark energy, named to reflect its mysterious nature, causes the observed accelerating expansion of the universe (Riess et al. 1998). They seek to measure its equation of state, $w(z)$, which describes how its density relates to the pressure it exerts. A cosmological constant, as in Einstein's theory of general relativity, could explain it, meaning that $w(z) = -1$, but various other models exist that predict different equations of state and produce unique expansion histories. As one goal of the survey, HETDEX seeks to constrain the form $w(z)$ can take by carefully measuring the Hubble constant, $H(z)$, and the angular diameter distance, $D_A(z)$ by using the size scale of the baryonic acoustic oscillations, which are characteristic distance scales imprinted on large-scale structure after recombination occurred. In order to detect dark energy at a minimum 3σ confidence level, HETDEX must cover a volume of 9 Gpc^3 with about 10^{-4} objects per Mpc^3 (Hill et al. 2004). Lyman-alpha emitting galaxies populate the universe ubiquitously over the ages observed, so they serve as a natural choice for tracing the expansion history.

Lyman-alpha Radiative Transfer

The Lyman-alpha photon serves as the most prevalent example of resonant scattering in the universe. Because the emission corresponds to the electron transition from the ground state to the first excited state of neutral hydrogen, and the vast majority of electrons in neutral hydrogen occupy the ground state in the cold-phase of the interstellar medium (ISM), one excited hydrogen atom can emit the photon only for it to get absorbed by another hydrogen atom which

shortly de-excites and reemits the same photon, so the chain of excitation and emission can continue repeatedly. Typically, the photon eventually collides with a dust grain instead of another hydrogen atom, and the dust grain extinguishes its energy (Berry et al. 2012). This explains why Lyman-alpha radiation faces such difficulty escaping from galaxies in order for Earth-bound observers to detect it at all. The process becomes increasingly complicated when considering the motion of the hydrogen atoms that absorb and emit the photon. An atom with some velocity sees the Lyman-alpha photon Doppler shifted by its motion, and, if the atom does absorb the photon, it re-emits the radiation in a random direction in its own rest frame. So, in most cases, the energy of the absorbed photon does not equal the energy of the reemitted photon, aiding in the radiation's escape from a cloud of hydrogen. For example, an expanding cloud of hydrogen favors the escape of Lyman-alpha radiation from the center with a slightly longer wavelength since the outward motion causes higher-energy photons to appear at the correct wavelength for absorption in the gas's rest frame (Dijkstra et al. 2006). Other emission lines do not face the same difficulty exiting their galaxy as Lyman-alpha radiation because they are not resonant transitions. Absorption lines originating from excited species like carbon, oxygen and silicon can therefore be used to measure any existing offset of Lyman-alpha emission from the galaxy's rest frame.

Previous Velocity Offset Measurements

Since LAEs appear extremely faint in HETDEX observations, measuring the locations of Lyman-alpha emission and various absorption features proves impossible. The only hope of performing such an analysis lies in stacking many spectra in order to amplify weak features in

individual spectra, and several astronomers have done this to analyze star-forming galaxies (SFGs) at high redshifts in recent years.

Alice Shapley and Charles Steidel performed a survey of Lyman Break Galaxies (LBGs) at z~3 (Steidel et al. 1996) and took spectroscopy on 1320 of the 2347 galaxies they found in total. In their study, long integration times allowed them to obtain spectra with Lyα emission and interstellar absorption for 40% of objects, and for 95% of this group, the redshift obtained from Lyα was higher than that obtained from the interstellar absorption features. On average, they found an offset of $\Delta v{\sim}650$ km s^{-1}. They theorized that large-scale outflows could create such a disparity, and LBGs harbor the rapid star formation rates capable of producing such outflows (Heckman 2002).

Michael Berry and colleagues also performed spectral stacking to study properties of continuum- and narrow-band-selected star-forming galaxies in a redshift range of $2 < z < 3.5$ found by the MUSYC collaboration. Of the objects they detected, thirty-two satisfied the equivalent-width requirement, $W_{Ly\alpha} > 20$Å to be classified as LAEs. They found an average velocity offset of $\Delta v{\sim}600$ km s^{-1} between Lyα emission and low-ionization absorption for all subsamples, with Lyα having a higher redshift than interstellar absorption in every case (Berry et al. 2012). They also determined that galaxies with larger $W_{Ly\alpha}$ tended to have weaker interstellar low-ionization absorption lines. In order to perform the measurement, Berry et al. divided their spectra into subsamples according to their Lyα equivalent widths, UV-colors, and redshifts.

Importantly, Berry at al. and Shapley et al. did not select their galaxy samples using the same technique as the HETDEX survey; they detected the continua of their objects as opposed to finding a single emission line as HETEDEX does. Generally, galaxies detected through their

emission lines tend to have lower stellar masses and lower dust attenuations in the optical and UV bands (Bowman et al. 2012). The different methods tend to select galaxies with disparate properties which could lead to significantly distinct offsets of Lyα emission from interstellar absorption. For example, if outflows driven by supernovae strengthen with increasing stellar mass, then the offset may be smaller on average for LAEs found in the HETDEX survey.

Chapter 2

Samples of Objects

In this section, I will briefly describe how the emission line detection catalog was developed by scientists on the HETDEX team, and I will also detail how I chose subsamples of likely LAEs to produce the various composite spectra.

The Detection Catalog

For my analysis, I utilized a catalog of 94,636 emission line detections found within HETDEX observations taken before March, 2019. The catalog includes information about each detection, such as the estimated central wavelength of the emission line, the Chi-squared statistic of the fit, the signal-to-noise of the line, the strength of the object's continuum, and more. Each detection entry has an associated spectrum with error estimates and information about the IFU fibers involved in the detection. Figure 1 shows an example of a typical detection from the catalog. As the figure shows, the survey hinges upon picking extremely faint features out of very noisy spectra, but HETDEX's carefully designed detection algorithm can do just that.

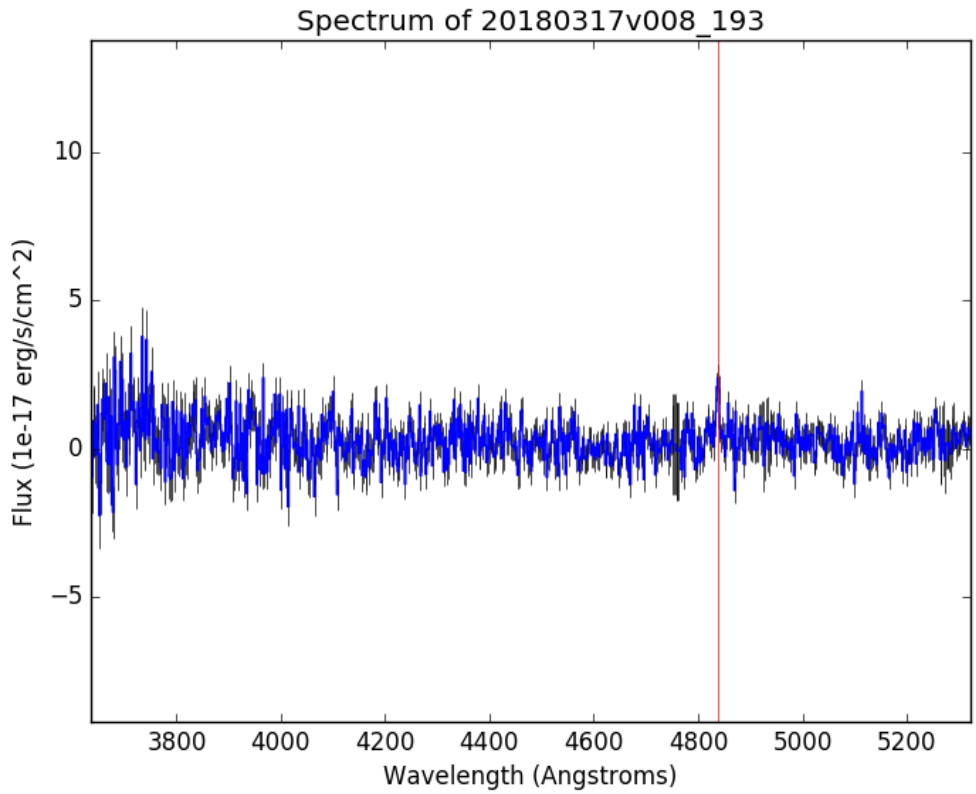

Figure 1 - Sample spectrum of possible HETDEX emission line galaxy

The detection algorithm follows a similar methodology to that developed during the HETDEX Pilot Survey (Adams et al. 2011). In that survey, the algorithm searched for excursions above 1σ significance in continuum-subtracted spectra with a 6 Å boxcar smoothing and created "seed" apertures, fitting a Gaussian profile to the possible line. Then, the algorithm searched the neighboring fibers for possible emission lines with the same central wavelength and width but varying intensity. The aperture grew as long as each added fiber contributed above some threshold of signal-to-noise and could reach a maximum size of six fibers since the dither pattern could cause a point source to be equidistant from that number at most. The algorithm that generated the detection catalog used in this analysis first performed the Gaussian fitting using ± 30 Å bins and accepted results with $SN_1 \geq 6.2$. They then fit a fixed 2.5" aperture on each of

these sources and looked for fibers within the aperture that had fits at the same wavelength with $SN_2 \geq 4.5$. The signal-to-noise parameters SN_1 and SN_2 were determined by simulating detections and finding the cutoff necessary to change the ratio of real sources to false detections in such a way as to minimize the uncertainties in estimating cosmological parameters.

Importantly, the algorithm does not address distinguishing LAEs from interloping galaxies at lower redshifts; any detected emission line enters the catalog. An example spectra of an obvious [OII]λ3727 galaxy contained within the catalog is shown below.

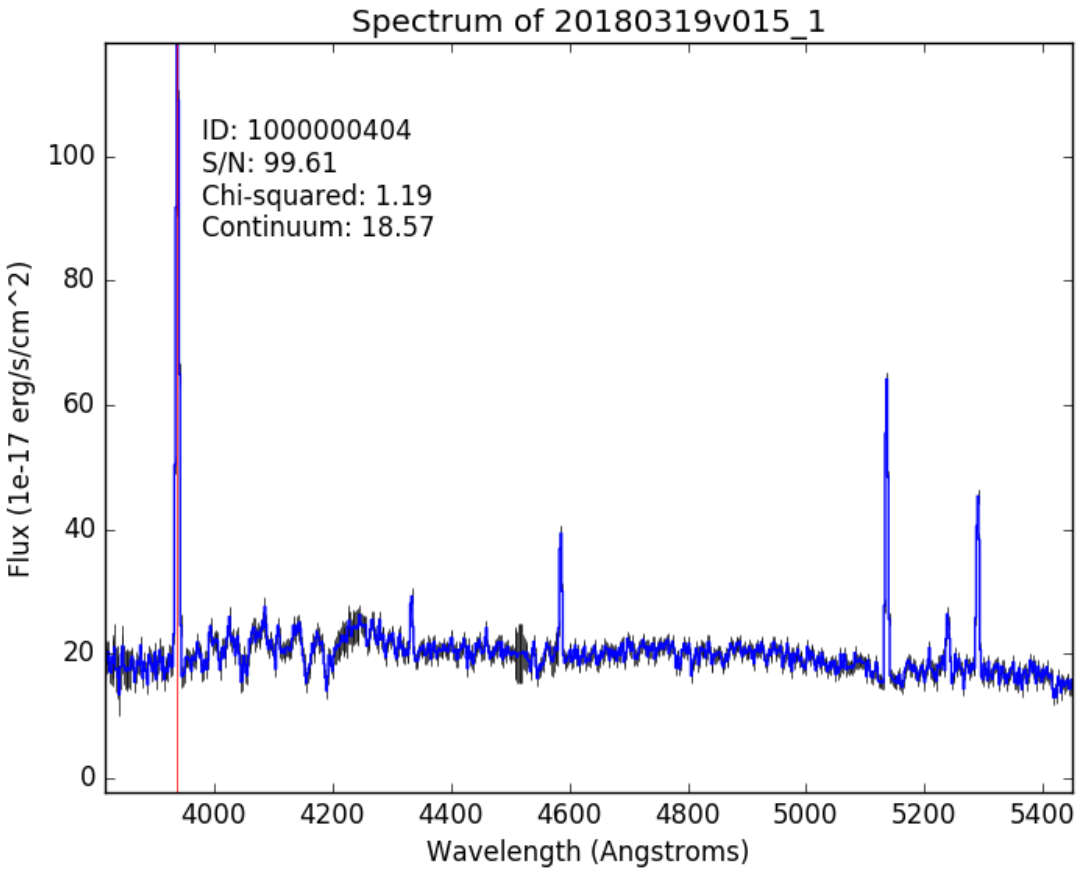

Figure 2 – Spectrum of an [OII] emitting galaxy at z~0.06

The strongest line pictured is [OII]λ3727, with next strongest being Hβ (4861 Å) followed by [OIII]$\lambda\lambda$5007,4959 which all correspond to a redshift of $z\sim0.06$. These spectra

stand out from LAEs because the signal-to-noise ratios of the detections are often very high (>20), the continuum is detected significantly, and multiple other emission lines exist within the spectrum. Culling the data with respect to these properties is one way to discriminate between the two types of objects. For example, for any supposed [OII] emission line detected at $\lambda \lesssim 4210$ Å, Hβ would also fall within the detectable wavelength range, and [OIII] would additionally appear for a detection at $\lambda \lesssim 4100$ Å. Nonetheless, the absence of the other lines for detections with wavelengths below the above thresholds does not conclusively prove the object is an LAE.

The Subsample of LAEs

Within the detection catalog are spectra with multiple detected emission lines and objects that are not LAEs at all, such as interloping [OII] emitting galaxies. To generate a reliable subsample, I studied the properties of the larger whole as well as the shortcomings of the detection algorithm.

Unsurprisingly, the algorithm struggles to make reliable detections toward the blue end of the wavelength range. Figure 3 shows an example of one such a false detection on the very edge. To remove these false detections from the subsamples, I made a histogram of the detection wavelengths so see if the algorithm failed with greater probability within certain wavelength ranges. As Figure 4 shows, detections occur with heightened frequency for wavelengths shorter than roughly 3600 Å. Importantly, this wavelength lies below the rest wavelength of [OII]λ3727, so the bump in detections arises solely from the detection algorithm struggling in the high signal-to-noise blue-end of the spectra.

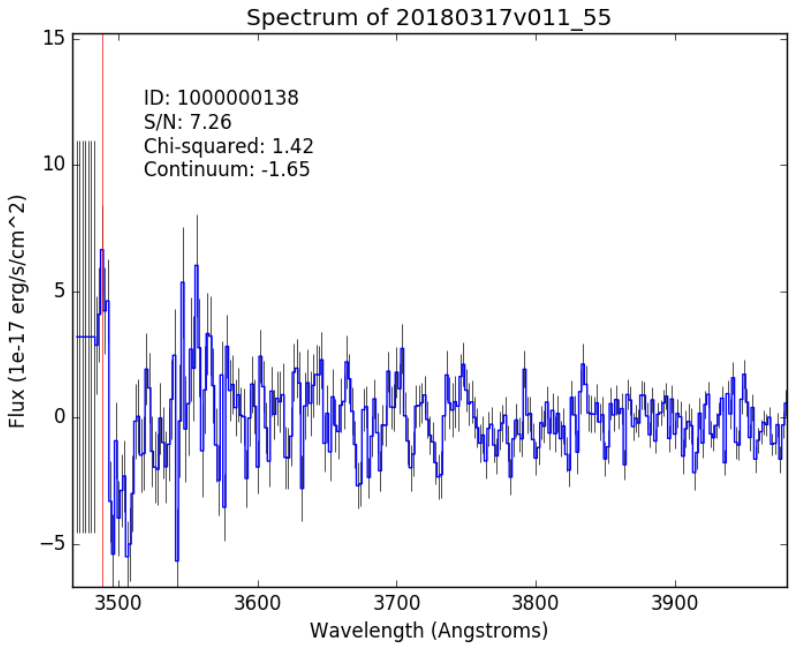

Figure 3 – False detection at the very edge of the wavelength range.

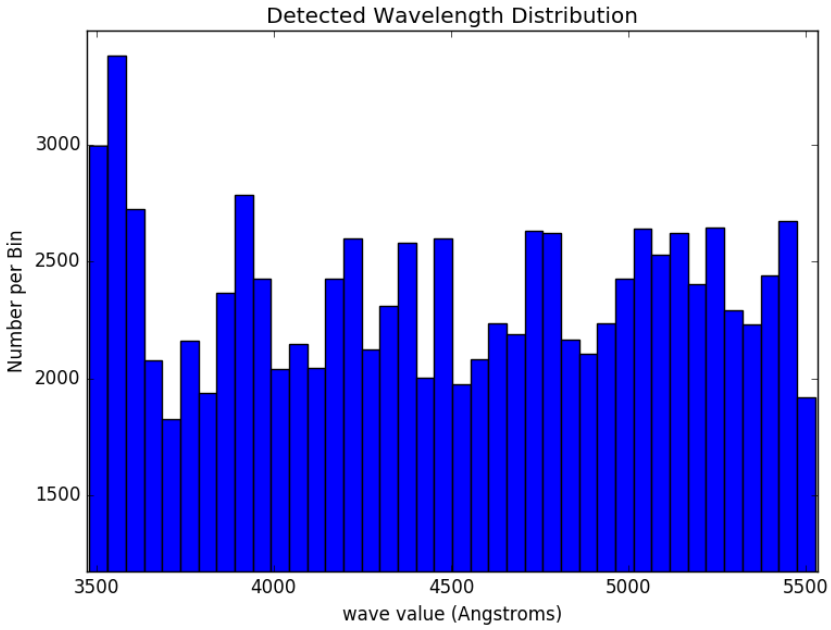

Figure 4 - Histogram of detected wavelengths

In general, I observed that objects with detections having signal-to-noise ratios greater than about twenty were invariably galaxies at low-redshift with non-zero continua and often multiple emission lines. In addition to placing an upper bound on signal-to-noise, I removed spectra with multiple emission lines present in the spectra. To do this, for any given subsample created by signal-to-noise, continuum, and detected wavelength cuts, I used the RA and DEC of the object to see if any entries in the subsample lay within a 2" radius of a different entry in the catalog. I chose this radius because, with the survey's current astrometric precision of 0.35" (Gebhardt et al. 2019), it ensures no object with multiple emission line detections gets overlooked.

Chapter 3

Methodology

In order to combine the spectra, I had to develop code that worked efficiently and accurately to produce composite spectra with contributions from as many as tens of thousands of individual objects. In this section, I explain the procedure I developed to do this.

Combining Spectra

The first and most crucial step in combining the objects' spectra was establishing a common wavelength scale to transform them into. The effective spectral range of the VIRUS spectrograph is roughly 3500-5500 Å, so using the rest wavelength of Lyα, 1216 Å, I found the maximum possible extent of the rest-frame spectra.

$$\lambda_{obs} = \lambda_{em}(1 + z) \quad (3.1)$$

Using this relation, the instrument can detect the emission line over a redshift range of $z \approx 1.9 - 3.5$. Therefore, the shortest possible measurable rest-frame wavelength is roughly 780 Å and the greatest possible is about 1900 Å. Over this range, a rich variety of features exists from absorption by species in low- and high-ionization states. As an additional consideration, the observer-frame spectra of objects have a resolution of 2 Å, so at the average redshift, that resolution corresponds to about 0.6 Å. Instead of using this information to construct a linear wavelength scale from the shortest to longest observed rest wavelengths, I chose to use a logarithmic scale.

$$\log(\lambda_{obs}) = \log(\lambda_{em}) + \log(1+z) \quad (3.2)$$

Using this scale, any offsets in the redshift simply result in an additive translation of the rest-frame wavelength as opposed to stretches from multiplication. This proves especially useful considering that the greatest challenge encountered in analyzing this sample is discriminating between LAEs and interloping galaxies at lower redshifts, such as [OII] emitting galaxies. In that case, mistakenly measuring a redshift from a detected emission line that is not Lyα simply slides the entire spectrum of that object along the logarithmic scale, so the composite spectrum still readily reveals the presence of interloping galaxies.

Using galaxies emitting the [OII] doublet as an example ($\lambda_{[OII]} = 3727$Å), it is straightforward to determine where spectral features in [OII] galaxies would appear on the wavelength scale of LAEs. I will refer to the ratio of the wavelength of [OII] and the wavelength of Lyα as ξ. Subscripts containing LAE refer to quantities derived assuming a detected emission line is Lyα while subscripts containing [OII] refer to properties of [OII] emitting galaxies. The redshifts determined from each assumption are related by the ratio ξ.

$$\frac{1+z_{LAE}}{1+z_{[oII]}} = \xi \quad (3.3)$$

$$\log(1+z_{LAE}) = \log\left(1+z_{[OII]}\right) + \log(\xi) \quad (3.4)$$

This equation connects how the rest-frame (denoted with subscript "*em*" for "emitted") of [OII] galaxies relates to that of LAEs.

$$\log\left(\lambda_{em}^{[OII]}\right) = \log(\lambda_{obs}) - \log(1+z_{LAE}) + \log(\xi) = \log(\lambda_{em}^{LAE}) + \log(\xi) \quad (3.5)$$

Therefore, given a spectral feature that appears on the logarithmic scale of the LAE spectrum, it may in fact correspond to a feature in an [OII] emitting galaxy at a true wavelength given by the following equation.

$$\lambda_{[OII]}^{em} = \xi \exp[\log(\lambda_{LAE}^{em})] \quad (3.6)$$

To set the bin size in log space, I required that the logarithmic scale with a uniform bin size contain the same number of bins as the linear scale with the aforementioned bin size of 0.6 Å at the average redshift. To transform a detected object to the master logarithmic scale, I first converted the observed wavelength to the rest-frame using the wavelength of the assumed detected Lyα line and determined where it overlapped with the master scale. Then, the counts in each linear bin of observed wavelength had to be re-binned into the bins of the master logarithmic scale. I chose to preserve the flux within each bin such that summing the counts over the entire spectral range in either linear or log space would produce the same total. To do this, for a given bin from the master scale, I found the fractions of the observed-frame bins that fell within it and multiplied the counts in each of the bins by the fraction. For error propagation, scaling the counts by some fraction also scaled the errors by the same fraction, and adding counts resulted in adding errors in quadrature.

After shifting each spectrum to the rest-frame (assuming a Lyα detection), converting to log-space, and re-binning according to the master scale, I had to combine the spectra. To do this, I began adding each spectrum to a master spectrum having zero counts that followed the master wavelength logarithmic scale. I kept track of the number of objects contributing to each bin and divided the final accumulated counts per bin by that number. Again, the errors for the counts per bin added in quadrature, but by dividing by the number of objects at the end, the errors scaled roughly as $1/\sqrt{N}$.

Chapter 4

Analysis

In this chapter, I present several composite spectra made by generating the subsample of objects from the catalog in various ways. Most importantly, I discuss whether features in the spectra arise from interloping galaxies or LAEs.

Features to Investigate

I looked for all of the low- and high- ionization absorption lines found in the composite spectra of star forming galaxies studied by Berry et al. (2012). Additionally, I superimposed several features common in [OII] emitters at the redshift-corrected wavelengths using Equation 3.6. This method allowed me to quickly determine whether a given subsample was dominated by interlopers and whether any discernable features could possibly arise from combined spectra of LAEs. I used rest wavelengths of atomic transitions tabulated by the National Institute of Standards and Technology. Tables 1 and 2 show the names, rest wavelengths, and descriptions of each of the features investigated in the composite spectra.

Table 1 - Features of interest in composite spectrum of LAEs

LAE Line Name	Rest Wavelength (Å)	Description
Lyα	1216	HI emission/absorption
Lyβ	1026	HI emission/absorption
SiII	1192, 1260, 1527	Low-ionization absorption
SiII+OI	1303	Low-ionization absorption
CII	1335	Low-ionization absorption
FeII	1608	Low-ionization absorption
AlII	1671	Low-ionization absorption
SiIV	1394	High-ionization absorption
NV	1240	High-ionization absorption
CIV	1549	High-ionization absorption

Table 2 - Features arising from interloping [OII] emitting galaxies

[OII] Emitter Line Name	Rest Wavelength (Å)	Description
[OII]	3726, 3729	Low-ionization emission
[OIII]	4959, 5007	Moderate-ionization emission
Hβ-H12	4861,4341,4102,3970,3889, 3834,3797,3770,3749	HI emission/absorption
[NeIII]	3869	Moderate-ionization emission
K (CaII)	3934	Fraunhofer absorption
H (CaII)	3968	Fraunhofer absorption

In the subsequent plots, the two groups of features will be indicated with two different colored vertical lines at the expected rest wavelength assuming the detected line is Lyα (red) or [OII]3727 (green).

Composite Spectra

I start by presenting a composite spectrum that demonstrates the prevalence of [OII] emitting contaminants in the sample. To create the subsample, I restricted the signal-to-noise of detections to $8 < SN < 20$ because false detections become prevelant below the lower bound, and all objects I inspected above the upper bound were detections of foreground galaxies. The continuum was restricted to $-5.0 < continumm\ (1 \times 10^{-17}\ \mathrm{erg\ s^{-1}cm^{-2}}) < 5.0$ because the survey does not expect to detect continua of LAEs, but uncertainty in the estimation of the continuum can cause it to fluctuation in a small range around zero. The detection wavelength range was restricted to $3600 < \lambda(\text{Å}) < 5450$. The lower bound limits the increase in false detections toward shorter wavelengths, and the upper bound limits false detections at the red edge of the spectral range. Figure 5 shows the result of co-adding roughly 23,000 objects.

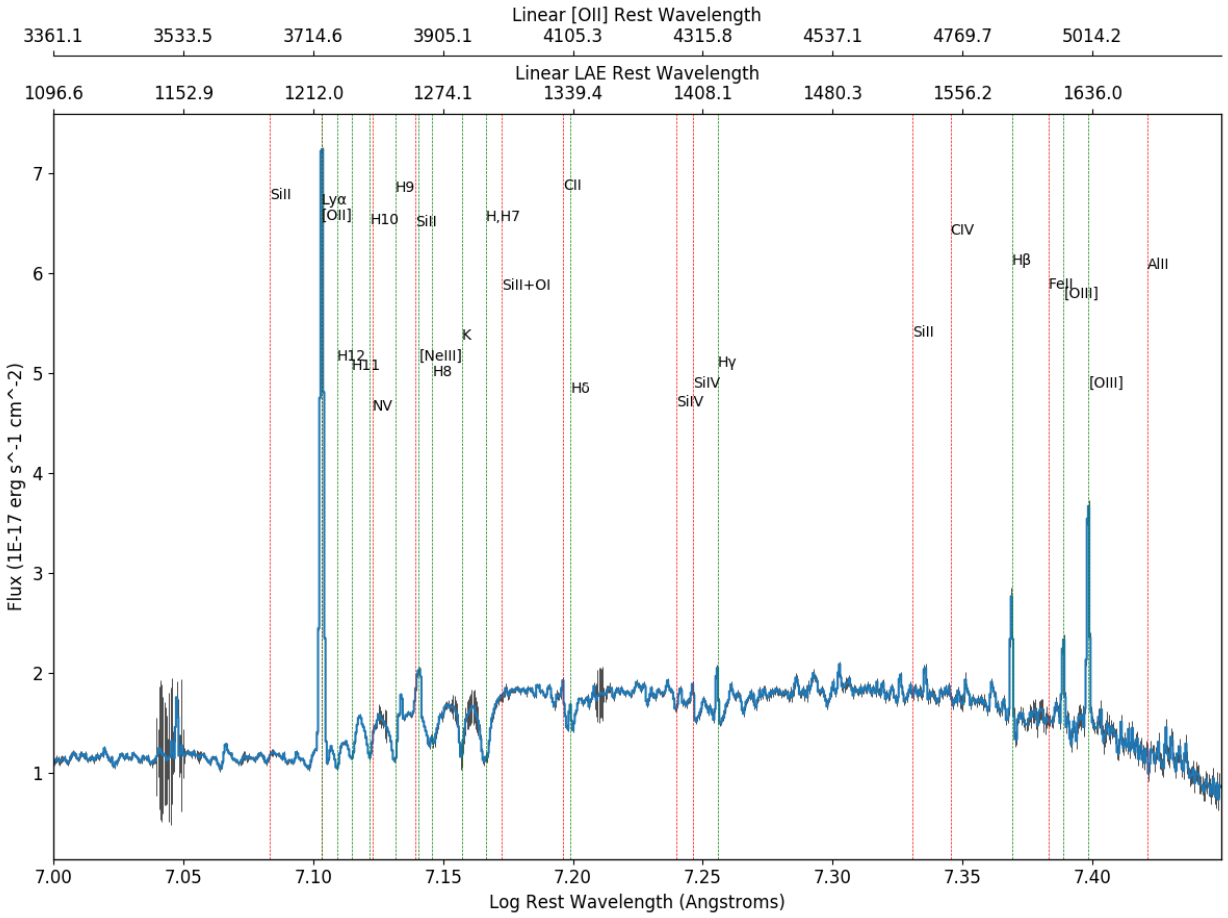

Figure 5 - Composite spectrum showing heavy contribution from [OII] emitting galaxies

The outstanding features in the spectrum are the intense Lyα/[OII] line (which must be present since the detected emission lines were assumed to be one of those features), the two [OIII] lines toward the red-end of the spectrum, and the prominent Hβ line. The latter features coincide perfectly with the wavelengths predicted when assuming the algorithm detected [OII] instead of Lyα. Figure 6 Presents a closer view of the spectrum just to the right of the Lyα/ [OII] line.

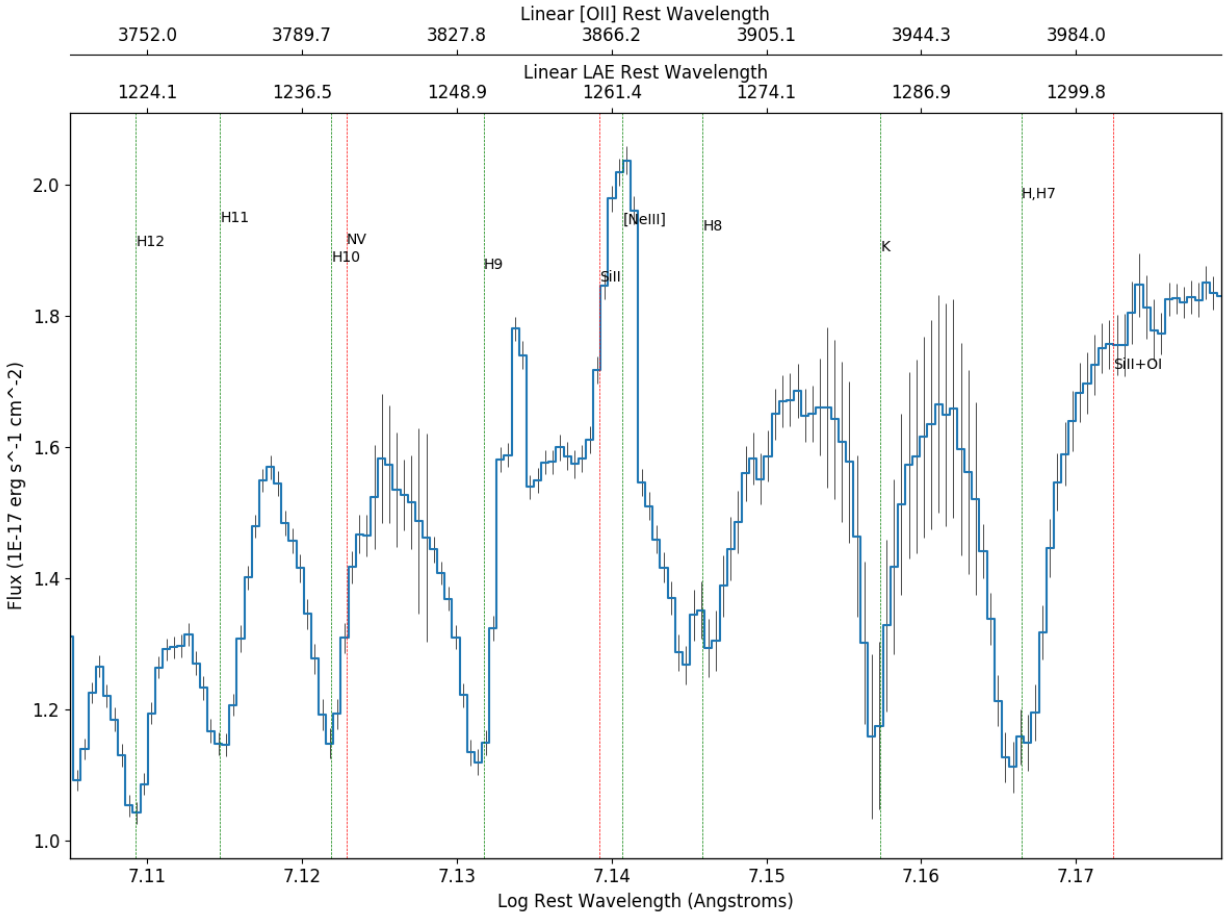

Figure 6 - Zoomed in view of Figure 5 showing clearly detected absorption from the Balmer series in [OII] emitting galaxies.

This region of the spectrum proves beyond doubt the prevalence of [OII] contaminants in the catalog. Every single Balmer transition beginning at $n = 7$ and going up to $n = 12$ appears at precisely the expected wavelength. The three possible LAE features within this spectral range do not convincingly align with any of the many absorption features. Additionally, this spectrum demonstrates the program's ability to co-add noisy spectra and extract a rich variety of features that would be extremely difficult to distinguish from a single object.

I also used the simplest method of avoiding [OII] contamination to see if any features very close to the Lyα line could be seen using a small sample of objects. I limited the wavelength range to $3600 < \lambda(\text{Å}) < 3720$ so that the [OII] emission line would not fall within the interval, and I used the same continuum and signal-to-noise cuts as in the previous spectrum. Figure 7 shows the resulting composite spectrum of 438 objects.

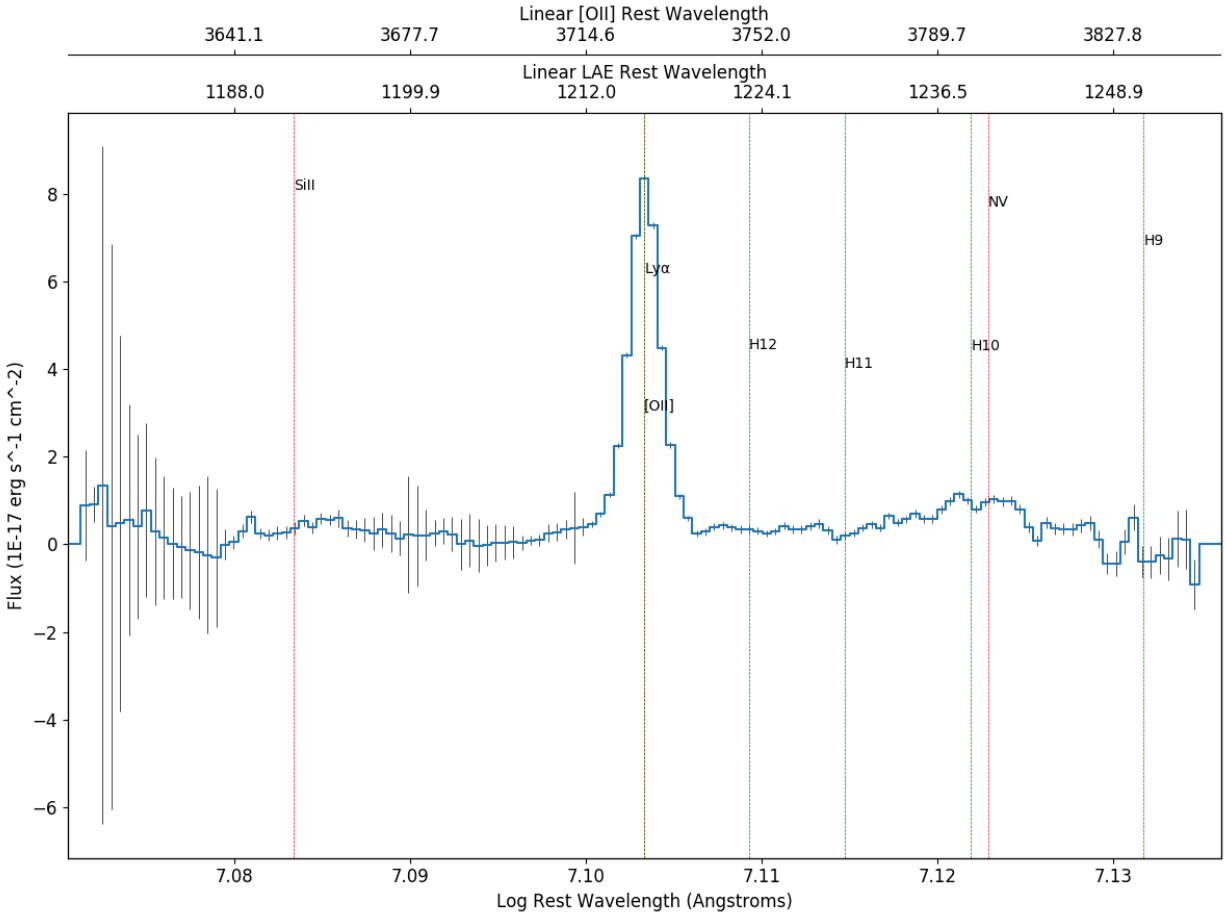

Figure 7 - Composite spectrum of 438 objects with detected wavelengths below [OII]λ3727. No convincing absorption lines appear in the spectrum due to the small sample size.

The two possibly observable features for this wavelength range, SiII and NV, do not appear convincingly in the spectrum. Unfortunately, the sample size resulting from using this method limits the potential for the absorption lines to overpower the noise.

As a final attempt, I used a large wavelength range from 3600Å to 5450Å, a signal-to-noise range of $8 < SN < 20$, and a restricted continuum range of $-2.0 < continumm\ (1 \times 10^{-17}\ \mathrm{erg\ s^{-1}cm^{-2}}) < 1.0$. Save for visually inspecting individual spectra or images, the signal-to-noise and continuum cuts are currently the only way to try to limit contamination from [OII] emitters. The resulting spectrum of 13,749 objects looks slightly better than the previous attempt that did not restrict the continuum strength as tightly, but interloping galaxies still dominate the signal.

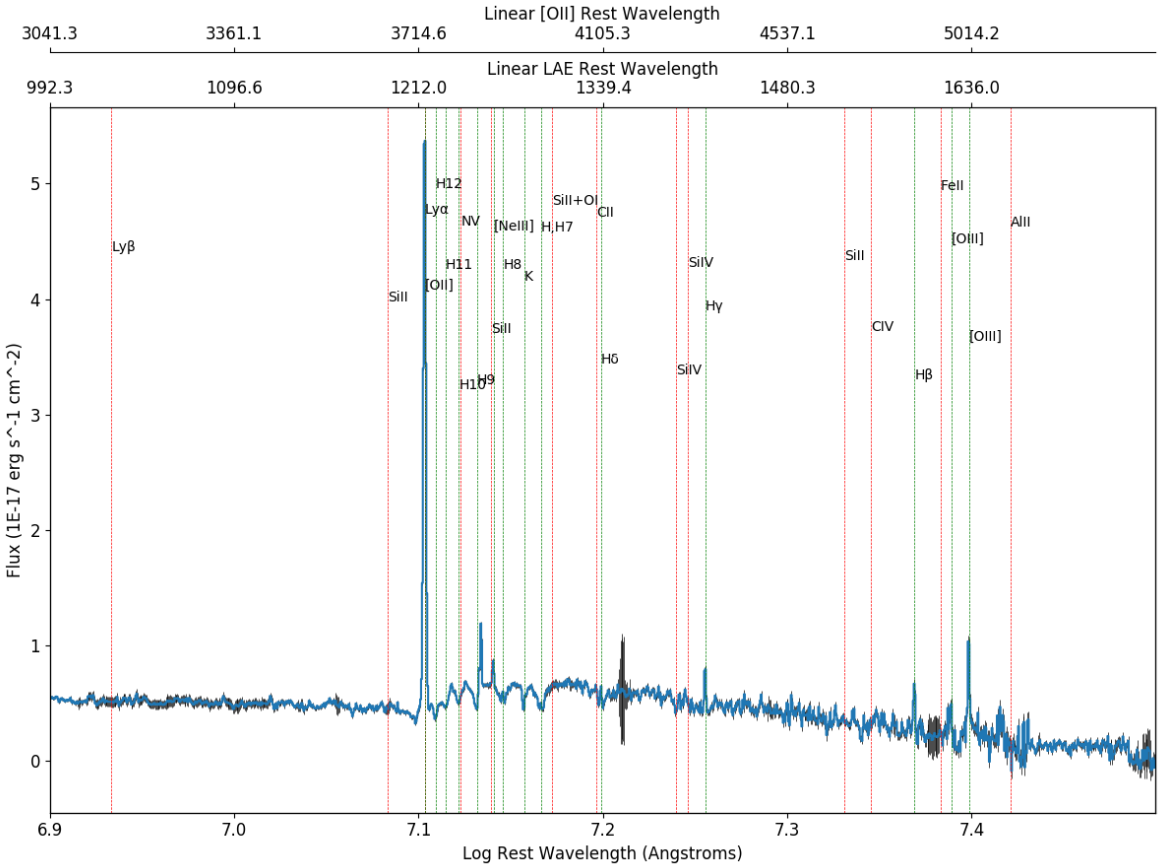

Figure 8 - Spectrum of subsample with strict continuum limits to reduce contamination from interlopers.

Unsurprisingly, the continuum level has dropped, but the strengths of the Lyα/[OII] and [OIII]5007 lines have also weakened substantially, indicating less contamination from interlopers. In this spectrum, I could only find two possible absorption features from LAEs in the subsample.

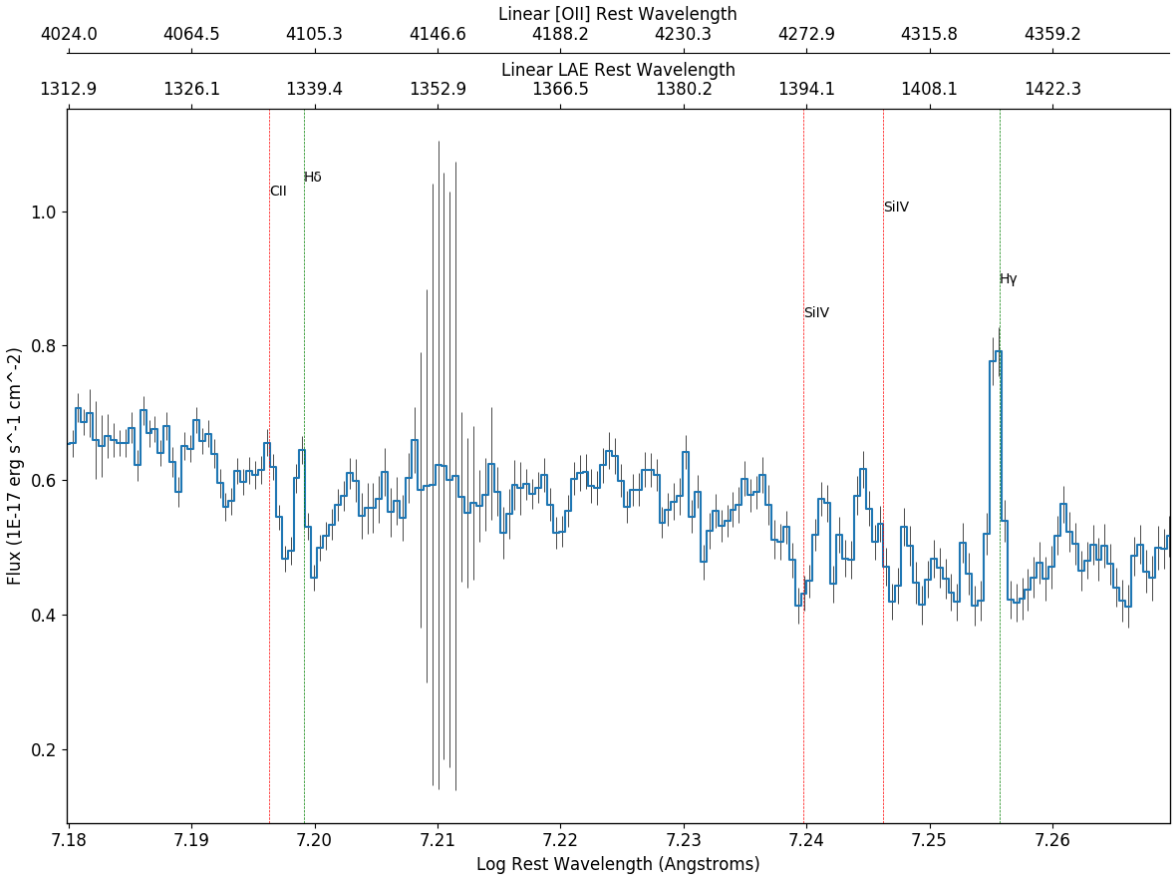

Figure 9 - Zoomed-in view of Figure 8 showing possible absorption from CII and SiIV in LAEs within the subsample.

In this wavelength range, there are three possible LAE absorption lines, one from CII and two from SiIV. The CII feature appears redder than predicted by the location of the Lyα line, but the shorter wavelength SiII line appears in the predicted location while the longer wavelength line appears redder. Moreover, the presence of Hδ complicates determining the existence of the CII line as it may absorb in its wings and emit at line-center. Given the noisy nature of the spectrum in general, many features look like absorption lines without corresponding to known atomic transitions, so verifying the presence of line absorption in LAEs within the subsample requires identifying many lines at or near the expected wavelengths. Although I was unable to

convincingly observe interstellar absorption lines in the composite spectra, the analysis I developed clearly succeeds in amplifying weak features in distant galaxies, and with better techniques for [OII] emitting galaxy discrimination, I am confident that this measurement can be made in the very near future.

Chapter 5

Conclusions and Outlook

For this analysis, I worked with a catalog of 94,636 HETDEX spectra of objects with significantly detected emission lines and used software I created to transform the spectra into their rest-frames with a logarithmic wavelength scale, re-bin them according to a master template spectrum while conserving flux, and co-add the spectra into one composite spectrum containing tens of thousands of objects. Unfortunately, my scientific goal of amplifying weak interstellar absorption features in the spectra of LAEs in order to measure their offset from the Lyα emission line was thwarted by the prevalence of low-redshift interloping galaxies in the catalog. For future work, one possible method to discriminate between LAEs and interlopers is to couple the detection with imaging data of the same location in the sky to determine if an object with a detectable continuum created the emission line. As HETDEX refines its detection algorithm, flux calibration, and sky subtraction, the data it collects will continue to improve in quality, and, after a concerted effort to remove interloping galaxies, I am confident the methodology described in this thesis will succeed in finding faint absorption features from LAEs to determine the velocity offset of Lyα due to large-scale galactic outflows.

BIBLIOGRAPHY

Adams, J.J., Blanc, G.A., Hill, G.J., et al. (2011). HETDEX Pilot Survey for Emission-Line Galaxies-I. Survey Design, Performance, and Catalog. *The Astrophysical Journal Supplement Series, 192,* p 5-40.

"Basic Atomic Spectroscopic Data Handbook." *The National Institute of Standards and Technology.* Sept 21, 2016.

Berry, M., Gawiser, E., Guaita, L et al. (2012). Stacked Rest-Frame Ultraviolet Spectra of Lyα-Emitting and Continuum-Selected Galaxies. *The Astrophysical Journal,749,* p 4-23.

Bowman, W.P., Zeimann, G.R., Ciardullo, R. et al. (2019). Galaxies of the z~2 Universe. 1. Grism-Selected Rest-Frame Optical Emission Line Galaxies. *Accepted to the Astrophysical Journal.*

Dijkstra, M., Haiman, Z., Spaans, M. (2006). Lyα Radiation from Collapsing Protoglaxies. I. Characteristics of the Emergent Spectrum. *The Astrophysical Journal, 649,* p 14-36.

Gebhardt, K., Ciardullo, R., Feldmeier, J. et al. (2019). Calibration, Commissioning, and First Sample of the Hobby-Eberly Telescope Dark Energy Experiment. *In prep.*

Heckman, T.M. (2002). Galactic Superwinds Circa 2001. *ASP Conference Series, vol 254,* p 292.

Hill, G.J., Gebhardt, K. Komatsu, E. et al. (2008). The Hobby-Eberly Telescope Dark Energy Experiment (HETDEX): Description and Early Pilot Survey Results. *ASP Conference Series, vol 399,* p 115.

Hill, G.J., Gebhardt, K. Komatsu, E. et al. (2004). The Hobby-Eberly Telescope Dark Energy Experiment. *The New Cosmology: Conference on Strings and Cosmology, AIP Conference Proceedings, vol 743,* p 224-233.

Hill, G.J., MacQueen, P.J., Smith, M.P. et al. (2008). Design, construction, and performance of VIRUS-P: the prototype of a highly replicated integral-field spectrograph for HET. *Proceedings of SPIE, vol 7014,* p 231.

Riess, A.G., Filippenko, A.V., Challis, P. , et al. (1998). Observational Evidence from Supernovae for an Accelerating Universe and a Cosmological Constant. *The Astronomical Journal, 116,* p 1009-1038.

Shapley, A.E., Steidel, C.C., Pettini, M., Adelberger, K.L. (2003). Rest-Frame Ultraviolet Spectra of z~3 Lyman Break Galaxies. *The Astrophysical Journal, 588,* p 65-89.

Steidel, C.C., Giavalisco, M., Dickinson, M., et al. (1996) Spectroscopy of Lyman Break Galaxies in the Hubble Deep Field. *The Astronomical Journal, 112*, p 352-358.

ACADEMIC VITA

Education

August 2015 - May 2019

- The Schreyer Honors College at The Pennsylvania State University
- Double Major: Astronomy and Astrophysics (with Honors), Physics
- Minors: Math, Spanish

Awards

2016

- The President's Freshman Award
- Academic Excellence Scholarship

2017

- The Sparks Award
- Astronomy Department Kadtke Scholarship
- Elsbach Honors Scholarship in Physics
- Academic Excellence Scholarship

2018

- The Evan Pugh Scholar Senior Award
- Academic Excellence Scholarship
- Mercedes T. Richards Memorial Scholarship
- The J & E Teas Science Scholarship

Research

- Penn State HETDEX Group, advised by Robin Ciardullo
- Spectroscopy software development, advised by Michael Eracleous

Teaching

- Learning Assistant (Penn State), ASTRO 291 & 292 - The Solar System and Astronomy of the Distant Universe, mentored by Donald P. Schneider

Publications

- Bowman, W.P., et al. "Galaxies of the z~2 Universe. IR Grism-Selected Rest-Frame Optical Emission Line Galaxies." *Accepted for Publication by the Astrophysical Journal.*

- Zeimann, G.R., et al. "Dust Attenuation and Emission in Distant Galaxies. I. Code Verification in Emission Line Galaxies at z ~ 2." *In preparation.*

Presentations

- **"**SpecOp: An Optimal Spectral Extraction Program for the Hobby- Eberly Telescope's LRS-2" *Poster.* Presented at the 231st meeting of the American Astronomical Society, 2018 Jan. 9, Washington, D.C.